Solar RRL
www.solar-rrl.com

Imaging Surface Recombination Velocities of Grain Boundaries in Multicrystalline Silicon Wafers via Photoluminescence

Hang Cheong Sio, Sieu Pheng Phang, and Daniel Macdonald*

We present a method for determining the effective surface recombination velocity (S_{GB}) of grain boundaries in silicon wafers, based on the photoluminescence contrast of the grain boundary and numerical modeling of the luminescence signal. It is found that in single-side passivated wafers, the luminescence contrast of a grain boundary is insensitive to lifetime variations in the neighboring grains, and hence can be directly correlated to S_{GB}. In combination with pattern recognition methods to locate the grain boundaries, this allows the S_{GB} of every grain boundary within a photoluminescence image to be explicitly determined and imaged.

High performance (HP) multicrystalline silicon (mc-Si) material is now becoming the mainstream material for mc-Si solar cell production. Owing to the significant reduction of dislocation clusters and the increased presence of grain boundaries (GBs) in the material, the cell efficiency of HP mc-Si solar cells may be strongly affected by recombination at GBs. The recombination behaviors of GBs are complex. Previous work has shown that the recombination properties of GBs can vary greatly between different mc-Si ingots,[1,2] along different positions of the same mc-Si ingot[3,4] and across the same mc-Si wafer,[5] and their behaviors depend on various parameters such as the geometry of the GBs,[5–7] the impurity level,[5] and the thermal history of the material.[2–4,8,9] A rapid, accurate, and reliable method for imaging the recombination activities of GBs is therefore desirable, in order to study their recombination behaviors and evaluate their detrimental impact on the final cell performance.

The majority of previous studies[1,4,5,7–9] have used signal contrast to evaluate and compare GBs. Signal contrast is defined as the intensity ratio of a measured signal at the GB and at the intra-grain region, with the signal usually derived from light- or electron-beam-induced current (LBIC, EBIC) or luminescence measurements. It is straightforward to measure and calculate, and thus allows a large number of GBs to be studied, which is important for statistically relevant analysis, given the large variation in GB behaviors.[3] However, the signal contrast method only provides a relative and qualitative representation, and strongly depends on the lifetimes of the intra-grain regions. This prohibits a direct comparison of results from different studies and across sample sets.

In order to obtain a more accurate evaluation of GB properties, various other works have described the recombination properties of a GB in terms of its effective surface recombination velocity (S_{GB}), and proposed methods for extracting this parameter based on analytical modeling and data fitting.[10–13] These methods provide a quantitative measure of the recombination properties of a GB. However, these methods usually involve time-consuming analysis and fitting routines, and hence the sample size is often limited.

In our previous work,[14] we demonstrated an approach to determine S_{GB} of a GB by fitting the PL intensity profile across a GB with a simulated PL profile, calculated with numerical modeling and a knowledge of several sample parameters, such as the intra-grain lifetime. An example of the fitting is demonstrated in **Figure 1**. In this work, based on the same model, we present a method to estimate S_{GB} of a GB simply based on the PL intensity contrast extracted from a PL image of a single-side passivated sample with a thin metallic film on the rear surface. The method is then combined with pattern recognition of GBs in PL images, to allow S_{GB} of individual GBs in large mc-Si samples to be spatially imaged.

Experimental details: The PL images in this work were captured using a BT Imaging LIS-R1 tool. An 808 nm laser was used for carrier excitation and the resulting band-to-band PL radiating from the samples was captured by a one megapixel silicon charge-coupled device (CCD) camera. Two imaging lenses with different magnifications were used in this study: a standard lens with a pixel resolution of around 163 μm and a high magnification lens with a pixel resolution of around 22 μm. A short pass filter with a cut-off wavelength at 1025 nm (for the standard lens) and 1050 nm (for the magnification lens) were fitted within the imaging lenses to reduce the impact of lateral light scattering both within the sample itself and within the camera's CCD chip, which cause blurriness in the acquired PL images at sharp features. Image deconvolution using an experimentally determined point-spread function (PSF)[15] was applied to the PL images to further reduce the impact of image blurring caused by crosstalk in the CCD chip.

The mc-Si wafers selected for this work were cut from a commercially grown p-type boron-doped high performance mc-Si ingot. Phosphorus-diffused samples were chosen due to the

H. C. Sio, S. P. Phang, D. Macdonald
Research School of Engineering,
The Australian National University, Acton,
ACT 2601, Australia
E-mail: kelvin.sio@anu.edu.au

DOI: 10.1002/solr.201600014

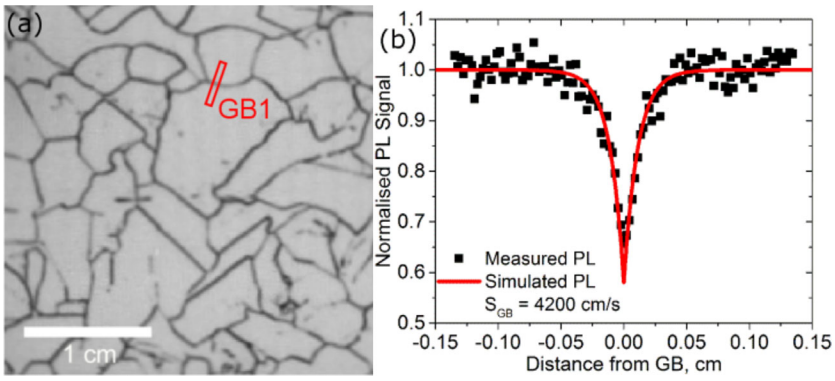

Figure 1. (a) PL images of a single-side passivated mc-Si wafer. The sample has been gettered via phosphorus diffusion. (b) Simulation fitting of GB1, as highlighted in (a). The PL profile is normalized against the PL signal in the intra-grain region far from the GB. The sample is illuminated with an incident photon flux of $2.1 \times 10^{17}\,cm^{-2}\,s^{-1}$ at 808 nm.

fact that GBs tend to be more recombination active after phosphorus gettering,[3] allowing a more clear demonstration of the method. After diffusion, the wafers were chemically etched to remove the phosphorus-diffused layer. The wafers then received silicon nitride films on the front surfaces for passivation, and thin metallic aluminum films on the rear surfaces using metal evaporation. The thin metallic aluminum films ensure instantaneous surface recombination conditions are achieved at the rear surfaces,[16] removing the necessity of determining the exact values of the surface recombination velocities of the rear surfaces, as would be required for the modeling[14] if using as-cut wafers.

Method description: In general, the PL contrast of a GB depends on the pixel resolution of the PL image, S_{GB} of the GB, the incident photon flux, the reflectivity, thickness, and doping of the sample (dopant type and concentration), the surface recombination velocities at the front and rear surfaces and the lifetime of the neighboring grains forming the GB. In double-side passivated samples that are commonly used for studying GBs, the PL contrast is strongly sensitive to the variation of the bulk lifetime in the intra-grain regions, which is difficult to measure accurately due to extensive lateral carrier diffusion. This dependence, however, is dramatically reduced in single-side passivated samples with infinite surface recombination at the rear surfaces.

Figure 2 shows simulated values of PL contrast as a function of S_{GB} in double-side and single-side passivated samples, determined with numerical simulations based on the model presented in Ref. [14]. As opposed to the double-side passivated sample, it can be seen that PL contrast is immune to lifetime changes in the intra-grain region in the single-side passivated sample, as long as the lifetime is above 50 μs, which is very often the case for modern mc-Si materials.[2] This is because the carrier concentration in the neighboring grains in the latter case is limited by carrier diffusion to the rear surface, due to the infinite rear surface recombination velocity. Since the PL contrast is almost independent of the intra-grain lifetime, it is possible to directly correlate it with S_{GB}, and to discriminate S_{GB} values up to $40{,}000\,cm\,s^{-1}$. Moreover, owing to the instantaneous surface recombination at rear, the PL contrast is also insensitive to the surface recombination velocity of the front surface as long as it is below $100\,cm\,s^{-1}$, allowing the approach to be applied on samples passivated with different surface passivation methods. Based on numerical simulation, varying the bulk lifetime from 50 μs to 1 ms would lead to a maximum variation of 3% in the PL contrasts, resulting in an error of less than 15% in the extracted S_{GB} values. Similarly, varying the recombination velocity of the front surface from 0 to $100\,cm\,s^{-1}$ would lead to a maximum variation of 2% in the PL contrasts, resulting in an error of less than 8% in the extracted S_{GB} values.

The correlation shown in Figure 2 depends only on measurement and sample parameters such as the spatial resolution of the PL image, the incident photon flux, the doping and thickness of the sample, which can be assumed to be uniform across an entire mc-Si sample. This allows the same correlation to be applied to convert the PL contrast of every GB in a mc-Si wafer into its corresponding S_{GB}, significantly reducing the modeling time required as compared to the direct fitting approach.[14]

Note in Figure 2 that the correlation between PL contrast and S_{GB} for the single-side passivated case is slightly affected by variation in the sample thickness (from 180 to 170 μm), especially at GBs with high S_{GB}. This induces some uncertainty in the method when applied on samples with large thickness

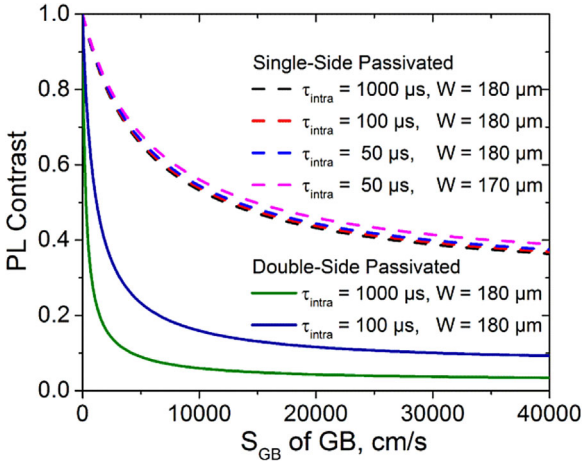

Figure 2. PL contrast of a GB as a function of S_{GB} in a double-side passivated and single-side passivated sample. PL contrast is defined as $PL_{GB}/PL_{intra\text{-}grain}$, where PL_{GB} and $PL_{intra\text{-}grain}$ are the PL intensity at the GB and at region far from the GB, respectively. Samples, with a background doping $1 \times 10^{16}\,cm^{-3}$, are assumed to be illuminated with an incident photon flux of $2.1 \times 10^{17}\,cm^{-2}\,s^{-1}$ at 808 nm. It was assumed that negligible surface recombination occurs at the passivated surfaces. The surface recombination velocities at the rear surfaces for the single-side passivated samples are assumed to be $3 \times 10^{6}\,cm\,s^{-1}$. The pixel resolution of the PL image is 163 μm.

variation. However, such uncertainties are expected to be small on typical industrial processed mc-Si wafers, and can be minimized with additional care in sample preparation. Moreover, the proposed method is also applicable to n-type mc-Si samples, since the difference in the carrier mobility can be easily accounted for in the modeling.

It should be noted that the PL contrast also depends on the spatial resolution of the PL image. For a given GB, its PL contrast reduces as the pixel size of the PL image increases. This has been taken into consideration in the modeling when calculating the detected PL signal in each camera pixel. This effect can be observed in Figure 2, in which the selected pixel resolution of the PL image (163 μm) limits the maximum PL contrast to around 0.35 for the single-side passivated samples.

Method verification: In order to verify the accuracy of the proposed method, we selected 22 GBs from a mc-Si wafer and compared their S_{GB} values extracted based on their PL contrasts using the approach outlined above, with those determined by the more complex direct fitting method presented in Ref. [14]. The result is shown in **Figure 3**. For the proposed method, the PL contrast was extracted from PL images acquired using a standard imaging lens, with a pixel resolution of around 163 μm. For the direct fitting method, a high magnification lens, with a pixel resolution of around 22 μm, was used to extract the PL profile. We chose to compare results obtained with lenses with different magnifications because the standard lens allows the method to be applied to a full 6 inch industrial mc-Si wafer, which is not achievable with the high magnification lens, while the high magnification lens, in principle, yields a more accurate determination of S_{GB} when using the direct fitting method. In order to reduce the measurement noise, we used the average PL profile over a segment of the GBs (around 800 μm in length) for both the fittings and the calculation of PL contrasts.

Figure 3 shows that most of the S_{GB} values extracted from both methods agree reasonably well with each other. A maximum discrepancy of around 40–50% is observed on some GBs. The discrepancy might be due to measurement noise, lateral variation of S_{GB} along the same GB, optical artefacts such as the sharpness of the imaging lens, or cross-talk in the silicon detector that is not fully corrected for. Since our proposed method strongly relies on the local PL intensity at the GB, it is more sensitive to such measurement artefacts as compared to the direct fitting approach, in which the entire PL profile across a GB is fitted. Nevertheless, the overall discrepancy is small when a large number of GBs is considered, and there is no systematic tendency to over- or underestimate the S_{GB} value. The overall difference in the average S_{GB} values among the 22 studied GBs extracted from both methods is less than 10%, indicating the validity of the proposed method.

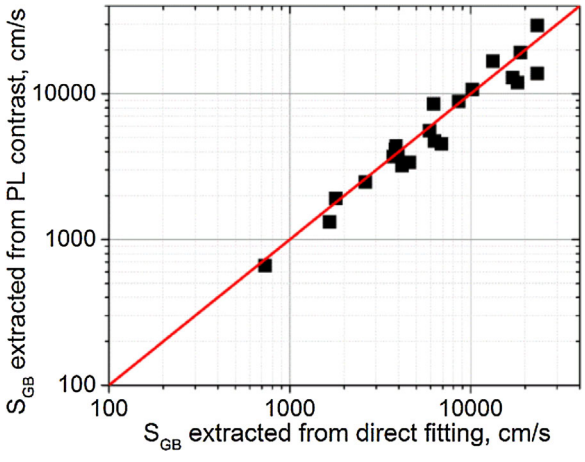

Figure 3. S_{GB} of 22 selected GBs extracted based on the PL contrast and direct fitting method presented in Ref. [14].

Results: The proposed method can be combined with pattern recognition of GBs in PL images, to allow S_{GB} of every GB in a mc-Si wafer to be determined and displayed as an image. **Figure 4** demonstrates the application of the S_{GB} imaging technique on a mc-Si wafer. In order to accurately calculate the PL contrasts for individual GBs within a PL image, it is critical to identify their exact locations within the PL image. In this work, we first applied the Canny method[17] using Matlab's inbuilt edge detection function to detect the presence of GBs. Afterwards, four line scans (vertical, horizontal, and two diagonal) were performed at each pixel at the detected locations and the exact coordinates of the GBs were then determined by searching the local minimum point along the line scans. The PL contrasts were

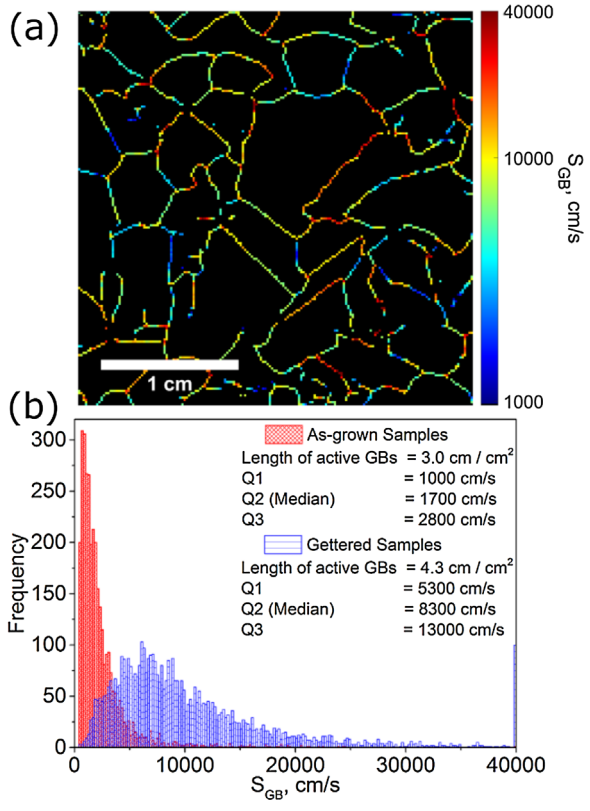

Figure 4. (a) S_{GB} map for the gettered mc-Si sample presented in Figure 1 (a). A logarithmic color scale is used in the figure. Intra-grain regions are denoted by black areas. (b) Histogram showing the overall statistics of S_{GB} in the gettered mc-Si wafer presented in (a) and an as-grown non-gettered sister wafer. Q1, Q2, and Q3 represent the first, second (median), and third quartiles of measured S_{GB} values, respectively. GBs with S_{GB} above 40,000 cm s^{-1} are attributed a S_{GB} value of 40,000 cm s^{-1}.

calculated using the local PL intensity at the GBs and the average PL intensity around the GBs, excluding the areas that were classified as GBs and those affected by them. For the modeling, we used the lifetime of an intra-grain region from a double-side passivated sister wafer. However, as mentioned above, the intra-grain lifetime has negligible influence on the results.

Figure 4(a) shows a corresponding S_{GB} map for the single-side passivated sample presented in Figure 1(a), derived using the proposed method. It can be seen that there is a large variation in S_{GB}, ranging from 500 to above 40,000 cm s^{-1}, within the studied mc-Si wafer. The overall distribution of S_{GB} is shown in Figure 4(b). There are approximately 4.3 cm of active GBs per square centimeter of the wafer in the studied mc-Si sample, and the active GBs have a median S_{GB} value of around 8300 cm s^{-1}. Note that the sample presented in Figure 4(a) has been gettered via phosphorus diffusion. For comparison, also shown in Figure 4(b) is the overall distribution of S_{GB} in an as-grown (non-gettered) sister wafer with the same surface treatments as the gettered wafer. It can be seen that phosphorus diffusion leads to an increase in the density of active GBs, as well as a very significant increase in the median S_{GB} value.

Here, we attributed a lower and upper detection limit of 400 and 40,000 cm s^{-1}, respectively, for S_{GB}. GBs with S_{GB} below 400 cm s^{-1} have a shallow PL profile and the reduction in the PL signal at the GB is comparable to the measurement noise. On the other hand, the dependence of S_{GB} on PL contrast starts to saturate when S_{GB} exceeds a certain value (around 40,000 cm s^{-1}), increasing the uncertainty of the method when applied on GBs with very high S_{GB}. The sensitivity of the method can be further improved by using PL images of higher spatial resolution, allowing GBs with $S_{GB} > 40{,}000$ cm s^{-1} to be discriminated. Nevertheless, we chose to use a PL image with a pixel resolution of 163 μm as it allows the method to be applied to 6 inch industrial wafers, while having a sufficient detection range to cover the vast majority of GBs in typical mc-Si samples, as shown in Figure 4(b).

It is worth noting that our model only accounts for two-dimensional carrier transport: carriers diffusing depth-wise and perpendicular to the GB. It assumes negligible diffusion of carriers radially around a GB and along a GB, as the carrier densities are assumed to not vary significantly in these directions. The assumption is generally valid for straight GBs with homogeneous S_{GB}, which describes the majority of the sampled GBs in Figure 4. However, this might induce some uncertainties at triple points, very bent GBs and dislocation clusters. The accuracy of the method could be further improved by implementing a more sophisticated three-dimensional model for such cases.

In conclusion, an approach for imaging S_{GB} based on PL imaging of single-side passivated mc-Si wafers is presented. This allows S_{GB} of every recombination active GB within a PL image to be explicitly determined, thus enabling the overall recombination behaviors of GBs in a mc-Si wafer to be statistically quantified in absolute scale. The method will allow quantitative comparisons of the recombination activities of GBs from different mc-Si materials, and assessment of the detrimental impact of GBs on the final solar cell performance.

Acknowledgments

This work is supported by the Australian Renewable Energy Agency (ARENA) under project RND009. The authors would like to acknowledge Jinko Solar for supplying the mc-Si wafers. H. C. Sio would like to thank D. Yan and E.C. Wang for assistance with sample preparation.

Received: October 20, 2016
Revised: November 15, 2016
Published online: December 7, 2016

[1] Karzel, P., Ackermann, M., Gröner, L., Reimann, C., Zschorsch, M., Meyer, S., Kiessling, F., Riepe, S., Hahn, G., *J. Appl. Phys.* **2013**, *114*, 244902.
[2] Sio, H. C., Macdonald, D., *Sol. Energy Mater. Sol. Cells* **2016**, *144*, 339.
[3] Sio, H. C., Phang, S. P., Trupke, T., Macdonald, D., *IEEE J. Photovolt.* **2015**, *5*, 1357.
[4] Joonwichien, S., Matsushima, S., Usami, N., *J. Appl. Phys.* **2013**, *113*, 133503.
[5] Chen, J., Sekiguchi, T., Yang, D., Yin, F., Kido, K., Tsurekawa, S., *J. Appl. Phys.* **2004**, *96*, 5490.
[6] Buonassisi, T., Istratov, A. A., Pickett, M. D., Marcus, M. A., Ciszek, T. F., Weber, E. R., *Appl. Phys. Lett.* **2006**, *89*, 042102.
[7] Stoffers, A., Cojocaru-Miredin, O., Seifert, W., Zaefferer, S., Riepe, S., Raabe, D., *Prog. Photovolt.* **2015**, *23*, 1742.
[8] Chen, J., Yang, D., Xi, Z., Sekiguchi, T., *Physica B: Condens. Matter* **2005**, *364*, 162.
[9] Takahashi, I., Usami, N., Mizuseki, H., Kawazoe, Y., Stokkan, G., Nakajima, K., *J. Appl. Phys.* **2011**, *109*, 033504.
[10] Donolato, C., *J. Appl. Phys.* **1998**, *84*, 2656.
[11] Corkish, R., Puzzer, T., Sproul, A. B., Luke, K. L., *J. Appl. Phys.* **1998**, *84*, 5473.
[12] Micard, G., Hahn, G., Zuschlag, A., Seren, S., Terheiden, B., *J. Appl. Phys.* **2010**, *108*, 034516.
[13] Riepe, S., Stokkan, G., Kieliba, T., Warta, W., *Solid State Phenom.* **2003**, *95*, 229.
[14] Sio, H. C., Trupke, T., Macdonald, D., *J. Appl. Phys.* **2014**, *116*, 244905.
[15] Walter, D. C., Liu, A., Franklin, E., Macdonald, D., Mitchell, B., Trupke, T., Proceedings of the 38th IEEE Photovoltaic Specialists Conference, **2012**, 307–312.
[16] Cuevas, A., Basore, P. A., Giroult-Matlakowski, G., Dubois, C., *J. Appl. Phys.* **1996**, *80*, 3370.
[17] Canny, J., *Trans. Pattern Anal. Mach. Intell.* **1986**, *8*, 679–698.